Photostable Zn_2SnO_4 Nanowire Transistors for Transparent Displays

Taekyung Lim,[†] Hwansoo Kim,[†] M. Meyyappan,[‡,§] and Sanghyun Ju[†,*]

[†]Department of Physics, Kyonggi University, Suwon, Gyeonggi-Do 443-760, Republic of Korea, [‡]NASA Ames Research Center, Moffett Field, California 94035, United States, and [§]Division of IT-Convergence Eng., POSTECH, Pohang, Republic of Korea

ABSTRACT

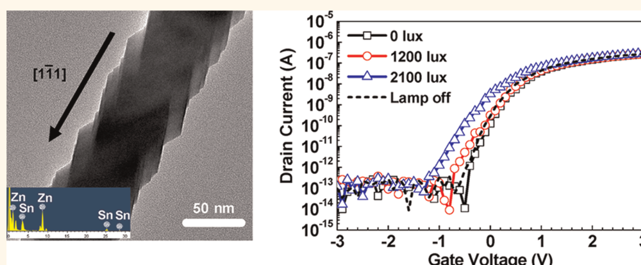

Although oxide nanowires offer advantages for next-generation transparent display applications, they are also one of the most challenging materials for this purpose. Exposure of semiconducting channel areas of oxide nanowire transistors produces an undesirable increase in the photocurrent, which may result in unstable device operation. In this study, we have developed a Zn_2SnO_4 nanowire transistor that operates stably regardless of changes in the external illumination. In particular, after exposure to a light source of 2100 lx, the threshold voltage (V_{th}) showed a negative shift of less than 0.4 V, and the subthreshold slope (SS) changed by ~0.1 V/dec. ZnO or SnO_2 nanowire transistors, in contrast, showed 1.5–2.0 V negative shift in V_{th} and an SS change of ~0.3 V/dec under the same conditions. Furthermore, the Zn_2SnO_4 nanowire transistors returned to their initial state immediately after the light source was turned off, unlike those using the other two nanowires. Thus, Zn_2SnO_4 nanowires achieve photostability without the application of a black material or additional processing, minimizing the photocurrent effect for display devices.

KEYWORDS: photostability · Zn_2SnO_4 · nanowire · transistors · display

Flexible, transparent displays have recently attracted much attention due to their mechanical flexibility in addition to optical transparency. These can be easily carried in a folded or rolled form or attached to clothing, and thus, the scope of potential applications is extensive including user-friendly forms as well as business and military applications. Recently, thin film and nanowire-based transistors using various materials including oxides have been reported for display applications.[1−5] While electrical characteristics desirable for each application have been studied carefully, device reliability critical in product development has not been addressed; the photocurrent of displays increases when the channel regions of the driving and switching transistors that drive the pixels are exposed to external light sources, thus leading to reliability issues. The increase in photocurrent can cause a positive or negative shift in the threshold voltage (V_{th}) and an increase in the leakage current. V_{th} variation exerts a critical influence on current change in displays. Displays consisting of basic circuits with two transistors–one capacitor (2T1C) exhibit considerable changes in current and picture quality due to V_{th} variation. Consequently, many studies have been conducted on circuit design compensating for the V_{th} variation. As for current change caused by V_{th} variation in the 2T1C structure, Lee *et al.*[6] indicated a 28% reduction in output current for about 0.2 V of V_{th} change with bias stress applied for 100 s. Additionally, Tai *et al.*[7] showed that a V_{th} variation of 0.33 V led to a 60% non-uniformity in output current. Park *et al.*[8] reported that displays were not able to realize uniform gray patterns due to the characteristic variation of transistors, but only red, green, and blue pixels were shown as randomly distributed images. These issues, in turn, could cause unstable picture quality and device operation, and therefore, a black matrix containing chromium (Cr) or carbon organic material is generally used as a color filter in thin film transistor liquid crystal displays to reduce the undesired effect of external light sources. In addition, many studies have attempted to minimize the photocurrent by various processes such as amorphous silicon (α-Si:H) back channel etching, Ar plasma treatment of the back surface, a bottom-gated metal light shield, and a self-aligned etch-stopper sidewall contact.[9,10]

Nanowires of wide band gap oxides such as ZnO, SnO_2, and In_2O_3 are suitable for flexible and/or transparent displays because they offer mechanical flexibility and optical

* Address correspondence to shju@kgu.ac.kr.

Received for review January 27, 2012 and accepted May 4, 2012.

Published online May 11, 2012
10.1021/nn300401w

© 2012 American Chemical Society

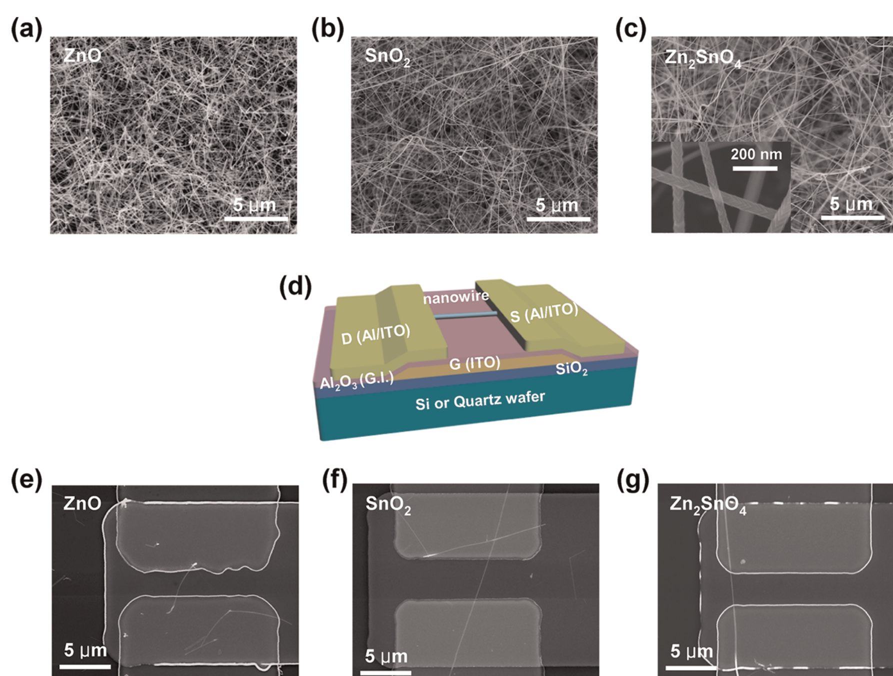

Figure 1. FE-SEM images of (a) ZnO, (b) SnO_2, and (c) Zn_2SnO_4 nanowires. The inset of (c) is the high-magnification image of Zn_2SnO_4 nanowires. (d) Cross-sectional view of the bottom-gated nanowire transistor. FE-SEM images of nanowire channel region for (e) ZnO, (f) SnO_2, and (g) Zn_2SnO_4 nanowire transistors.

transparency and can be processed at low temperatures. However, their characteristic response to light, which is helpful in photosensor applications, is a disadvantage in transistor applications for the reasons described above. Here, we have attempted to minimize the changes caused by external light through a compound oxide nanowire material that provides a stable device operation. We have synthesized Zn_2SnO_4 nanowires and investigated their crystallizability and semiconductor characteristics. A comparison of ZnO and SnO_2 nanowires shows that Zn_2SnO_4 nanowires produce stable electrical device performance regardless of the presence of external light sources without additional processing or increased cost.

RESULTS AND DISCUSSION

Figure 1a–c shows field emission scanning electron microscopy (FE-SEM) images of the ZnO, SnO_2, and Zn_2SnO_4 nanowires with average diameters and lengths of ~40 nm/~10 μm, ~40 nm/~20 μm, and ~50 nm/~15 μm, respectively. The nanowires exhibit zigzag patterns, as seen from the high-magnification image of Zn_2SnO_4 in the inset of Figure 1c. All three materials exhibit uniform growth patterns without flakes or dust. Figure 1d shows a cross-sectional view of the nanowire transistor device, and FE-SEM images of the channel area reveal that the channel diameters and lengths of representative ZnO, SnO_2, and Zn_2SnO_4 nanowire transistors are ~43 nm/2.8 μm, ~42 nm/5 μm, and ~52 nm/3 μm, respectively (Figure 1e–g).

Figure 2 shows the results of photoluminescence (PL) and X-ray diffraction (XRD) analyses of all three nanowires. The main XRD peaks for the ZnO nanowires appear at (100), (002), and (101), and they exhibit a hexagonal wurtzite crystalline structure with lattice constants a = 3.242 Å and c = 5.188 Å (ICDD No. 79-0205). The PL measurement (Figure 2d) shows a strong ultraviolet (UV) emission peak, green emission peak, and near-infrared (IR) emission peak at 379, 522, and 756 nm, respectively. These three peaks are generally found in ZnO thin films or nanostructures. The UV emission is widely known to be derived from the recombination of free excitons through exciton–exciton collisions caused by the wide direct band gap (3.26 eV) of ZnO.[11–13] The green emission around 500 nm is usually generated by deep-level defects in ZnO crystals such as oxygen vacancies, interstitial zinc, and interstitial oxygen.[11,14,15] Although the near-IR emission around 760 nm is sometimes thought to be caused mainly by interstitial zinc,[16] it is more likely to be the second peak of UV emission caused by transitions due to Si–O–Zn bonds.[12,17,18]

The XRD measurements for SnO_2 nanowires (Figure 2b) show main peaks at (110), (101), and (211), and the SnO_2 crystalline structure is tetragonal rutile with lattice constants a = 4.737 Å and c = 3.186 Å (ICDD No. 88-0287). In the PL spectrum (Figure 2e), UV emission at 382 nm and strong, broad yellow emission at 610 nm are observed. The peak at 382 nm is assumed to be generated below the shallow band of tetragonal SnO_2.[19] The yellow emission at 610 nm is attributed to defect levels in the band gap of SnO_2, which seem to have originated from defects during the growth phase.[20,21]

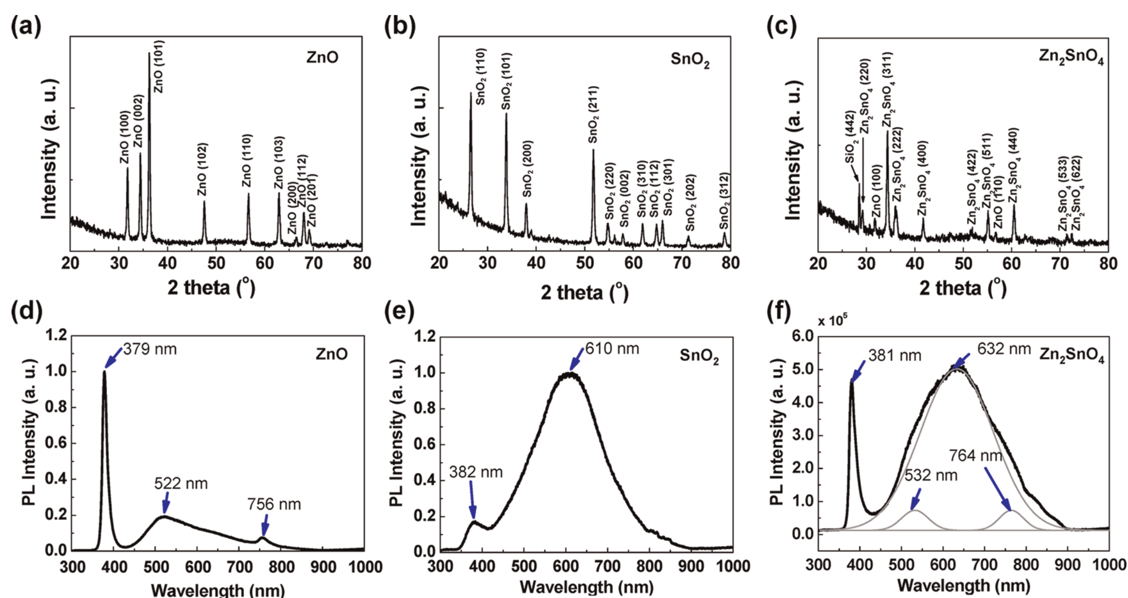

Figure 2. XRD spectra of (a) ZnO, (b) SnO_2, and (c) Zn_2SnO_4 nanowires. PL spectra of (d) ZnO, (e) SnO_2, and (f) Zn_2SnO_4 nanowires.

As shown in Figure 2c, the main XRD peaks for Zn_2SnO_4 are at (220) and (311), and the growth shows a cubic structure with a lattice constant a = 8.65 Å (ICDD No. 74-2184). In addition, SiO_2 and ZnO peaks are also observed on the background. The main cause of the ZnO peak is ZnO impurities generated during the synthesis as reported in other studies.[22−24] Nevertheless, it appears that the Zn_2SnO_4 nanowires are of excellent crystallizability here since the ZnO peaks are of low frequency and intensity. The PL spectra reveal two main peaks at 381 and 635 nm, as seen in Figure 2f. Previous reports on the PL of Zn_2SnO_4 revealed, in addition to a 360 nm peak, the band gap energy emission of Zn_2SnO_4, blue-green emission around 490 nm, orange-yellow emission around 600 nm, and red emission around 630 nm.[25−27] Although the origin of these PL peaks has not been clearly identified, they are reportedly associated with the Zn/Sn stoichiometry and oxygen vacancies. It is assumed that the characteristics of the Zn/Sn stoichiometry changed according to the ratio of Zn and Sn during synthesis of Zn_2SnO_4, and the PL peaks varied accordingly. A 381 nm peak, which is red-shifted by 2 nm from the UV emission peak of ZnO, is caused primarily by the band gap renormalization effect of mixed Sn.[27,28] The peak at 635 nm was proved to be the combination of three peaks at 532, 632, and 764 nm as derived by the Gaussian fitting. These peaks are considered to have been caused by an energy level formed within the band gap due to deficiencies such as oxygen, tin, and zinc vacancies generated in the spinel structure by the formation of Zn/Sn stoichiometry and the high point defect concentration during the synthesis process.[29−31]

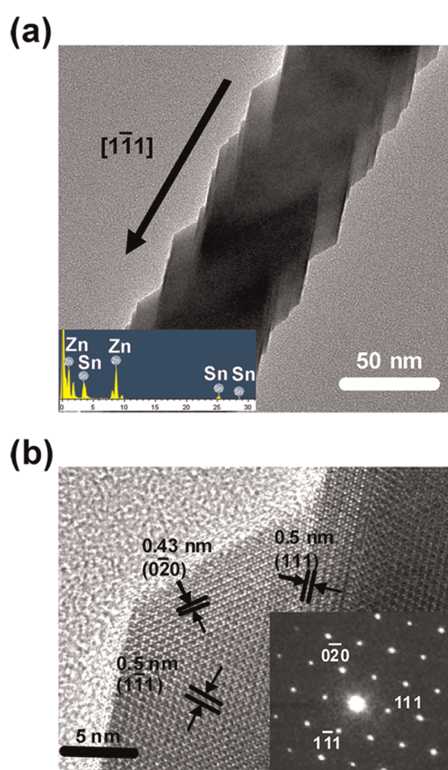

Figure 3. HR-TEM images of (a) Zn_2SnO_4 nanowire with an inset providing the EDS result and (b) side edge of Zn_2SnO_4 nanowire. Inset is the corresponding SAED pattern, taken along the [10−1] zone axis.

Figure 3 shows low- and high-magnification images from the high-resolution transmission electron microscopy (HR-TEM) analysis of representative Zn_2SnO_4 nanowires, which reveal that rhombohedral nanocrystals grew continuously along the nanowire axis.[32,33] The corresponding selected area electron diffraction

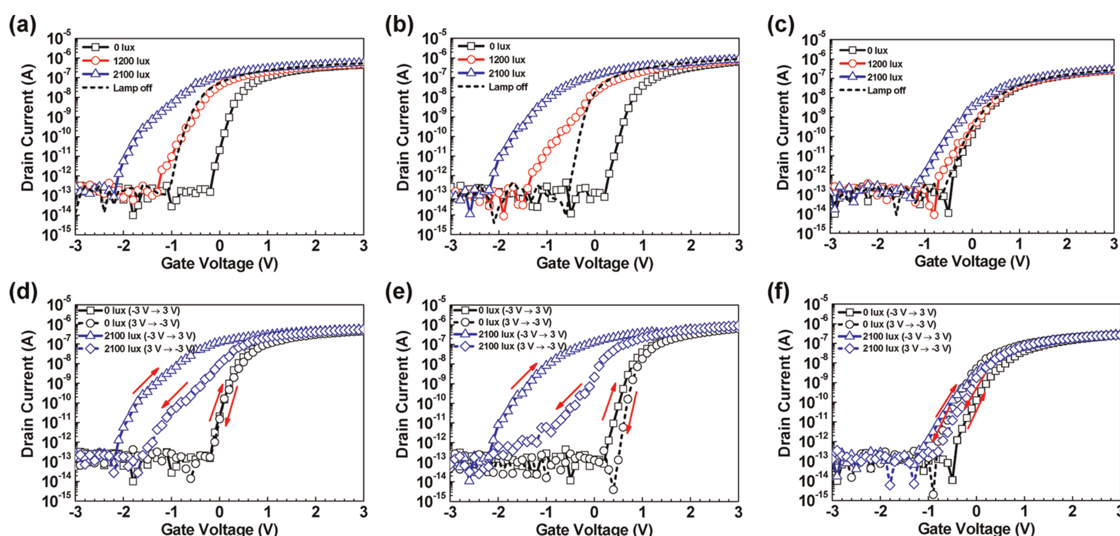

Figure 4. $I_{ds}-V_{gs}$ **characteristics of (a) ZnO, (b)** SnO_2**, and (c)** Zn_2SnO_4 **nanowire transistors under light intensities of 0, 1200, 2100 lx, and lamp off. Hysteresis characteristics of (d) ZnO, (e)** SnO_2**, and (f)** Zn_2SnO_4 **nanowire transistors measured at 0 and 2100 lx.**

(SAED) pattern (Figure 3b, inset) confirms the single-crystal nature of the Zn_2SnO_4 nanowires. According to the SAED pattern taken along the [10−1] zone axis, the growth orientation of the nanowires is [1−11]. The measured lattice spacing values of 0.50, 0.50, and 0.43 nm correspond to the (1−11), (111), and (0−20) planes of the spinel Zn_2SnO_4 nanowire, respectively. Energy-dispersive X-ray spectroscopy (EDS) in TEM (Figure 3a, inset) also confirms the Zn/Sn stoichiometry to be 67.35:32.65 (2:1).

Figure 4 shows the changes in the electrical characteristics of the ZnO, SnO_2, and Zn_2SnO_4 nanowire transistors under illumination. Three levels of illumination intensity were applied: 0, 1200, and 2100 lx. The most remarkable changes seen in the drain current *versus* gate-source voltage ($I_{ds}-V_{gs}$) characteristics of the ZnO nanowire transistors (Figure 4a) are a negative V_{th} shift and an increase in subthreshold slope (SS) with increasing illumination intensity. Specifically, V_{th} is 0.2 V at 0 lx, −0.54 V at 1200 lx, and −1.33 V at 2100 lx. The SS values are 0.14 V/dec at 0 lx, 0.25 V/dec at 1200 lx, and 0.39 V/dec at 2100 lx. Thus, V_{th} exhibits a negative shift of ~1.5 V, and the SS shows around 3-fold increase for an increase of 2100 lx in illumunation intensity. When remeasurement was performed with the lamp off, the slope remained on the same level as the initial characteristics (V_{th} = −0.63 V, SS = 0.15 V/dec), but V_{th} subsequently changed. Although the figure does not show it, V_{th} failed to completely return to its initial state even when it was measured after about 10 min. For a current with 0 V of gate bias, the increase in illumination intensity resulted in the same current increase from 21 pA at 0 lx to 121 nA at 2100 lx. However, this was generated by a negative shift in V_{th}. In other words, if we define V_{th} + 2.5 V as the on-current considering the shift in V_{th}, the on-current is approximately 300−400 nA; this was not increased or decreased by the photocurrent. Although the change in the $I_{ds}-V_{gs}$ characteristics according to the sweep direction of the gate voltage was very slight at 0 lx during hysteresis, a characteristic change occurred during illumination, exhibiting a positive shift in V_{th} of approximately 1 V when the sweeping direction was from −3 to 3 V compared to the other way around (Figure 4d).

SnO_2 nanowire transistors also showed a similar change in electrical characteristics with the photocurrent, as seen in Figure 4b. The V_{th} is 0.62, −0.39, and −1.36 V at illumination intensities of 0, 1200, and 2100 lx, respectively, showing a shift in the negative direction by ~2 V as the intensity is increased to 2100 lx. The SS values also increase from 0.11 V/dec at 0 lx to 0.37 V/dec at 2100 lx. In addition, V_{th} was −0.24 V and the SS was 0.11 V/dec when the lamp was off. If the external light source was removed, the slope returned to normal, whereas V_{th} was not restored to its initial state. For the current hysteresis characteristics shown in Figure 4e, the variation in V_{th} according to the sweep direction of the gate voltage increases from 0.15 V at 0 lx to 1.44 V at 2100 lx.

In contrast to ZnO and SnO_2 transistors, the change in Zn_2SnO_4 nanowire transistor under illumination is negligible, as shown in Figure 4c. V_{th} changes from 0.21 V at 0 lx to 0.17 V at 1200 lx and −0.17 V at 2100 lx, resulting in a negative shift of only −0.4 V. This result is outstanding compared to the shift of more than 1.5 V in ZnO or SnO_2. In addition, the SS changes from 0.25 V/dec at 0 lx to 0.35 V/dec under light illumination, an increase of only 0.1 V/dec. The hysteresis characteristics also scarcely show any change by the external light; the variation in V_{th} is 0.25 V at 0 lx and 0.3 V at 2100 lx depending on the sweep direction of the gate voltage (Figure 4f). In other words, the electrical and hysteresis

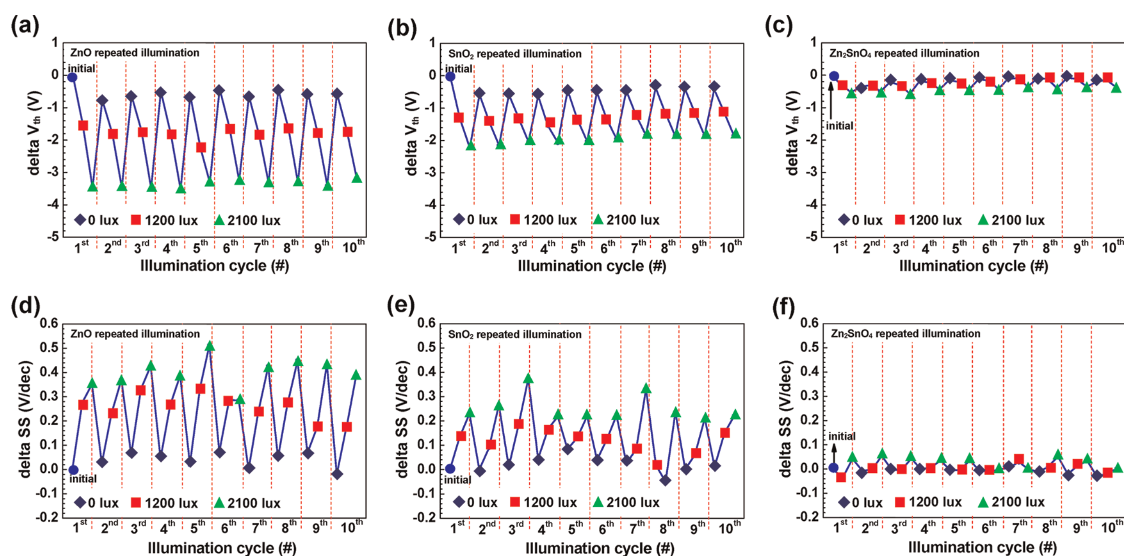

Figure 5. V_{th} **and SS changes of ZnO,** SnO_2**, and** Zn_2SnO_4 **nanowire transistors under 10 cycles of light illumination (0 lx−1200 lx−2100 lx−0 lx).**

characteristics are very stable compared to those of ZnO and SnO_2 nanowire transistors despite illumination by an external light source. The DC characteristics of the Zn_2SnO_4 nanowire transistors here with an on/off ratio of 2.1×10^6 and a field effect mobility (μ_{eff}) of ∼20 $cm^2/V \cdot s$ are better than reported values in the literature.[34,35] Here, the μ_{eff} was extracted from the gate-to-channel capacitance given by $C_i = 2\pi\varepsilon_0 k_{eff} L_{ch} / \cosh^{-1}(1 + t_{ox}/r_{nw})$ using $\mu_{eff} = dI_{ds}/dV_{gs} \times L_{ch}^2/C_i \times 1/V_{ds}$, where the effective dielectric constant of ALD-deposited Al_2O_3 (k_{eff}) is ∼9.0.

It is widely known that the main cause of photocurrent increase upon exposure to external light is photogenerated electron−hole pairs created under light illumination. Adsorption and desorption of oxygen molecules on the surface of nanowires is also thought to play a role on the photocurrent characteristics of ZnO and tin oxide.[34] Its strength depends on how processes such as carrier generation, charge trapping, and recombination interact with the deep-level defects and interface traps of the channel under light illumination. Thus, trapping of nanowires in a surface state can significantly affect carrier transport.[36−38] Under ambient and low-temperature conditions, oxygen adsorbs nondissociatively in molecular form either as neutral or negatively charged. The latter are formed by combining with the free electrons, thus reducing the electron concentration near the nanowire surface and the conductivity. Upon exposure to light, the photogenerated holes recombine with the negative ions on the nanowire surface and release the oxygen molecules, restoring the nanowire conductivity.[39] In order to verify whether the state of nanowire surface plays a major role in the change of photocurrent or not, we deposited Al_2O_3 (30 nm) onto a SnO_2 nanowire transistor for passivation and examined the changes with varied light illumination intensities. As illumination intensity increased from dark state (0 lx) to 1200 and 2100 lx, V_{th} changed to 0.42, −0.02, and −0.28 V, respectively. In other words, when light illumination increased by ∼2000 lx, V_{th} produced a 0.7 V negative shift. On the other hand, SnO_2 nanowire transistors without passivation exhibited a ∼2 V negative shift of V_{th} under the same conditions of light illumination, indicating a difference of 1.3 V. Meanwhile, the SS of passivated SnO_2 nanowire transistor was 0.21 V/dec in the dark state, 0.25 V/dec at 1200 lx, and 0.22 V/dec at 2100 lx, showing no outstanding change. Hence, the characteristic changes caused by varied illumination conditions significantly decreased because passivation did not allow the nanowire surface to react to atmospheric oxygen. Thus, the main reason for photocurrent generation is considered to be the adsorption and desorption of oxygen molecules existing on the nanowire surface.

Next we discuss the reason why *I*−*V* curves did not go back to their initial behaviors after the lamp was turned off. In general, atmospheric oxygen molecules are physically reabsorbed onto the nanowire surface when light illumination is removed. The molecules capture electrons from the conduction band and turn to chemisorbed oxygen, which leads to the reduction of photocurrent. Then, some part of the chemisorbed oxygen changes to physisorbed oxygen, whereas the rest remain as placed on the nanowire surface. It is well-known that ZnO is the main cause of long decay time due to its low physisorption rate.[40−42] However, Li *et al.* reported that the chemisorption rate is lower than the physisorption rate.[43] Taking these reports into consideration, it is assumed that restoration of the original state does not occur immediately after the lamp is turned off because the reabsorption of oxygen onto

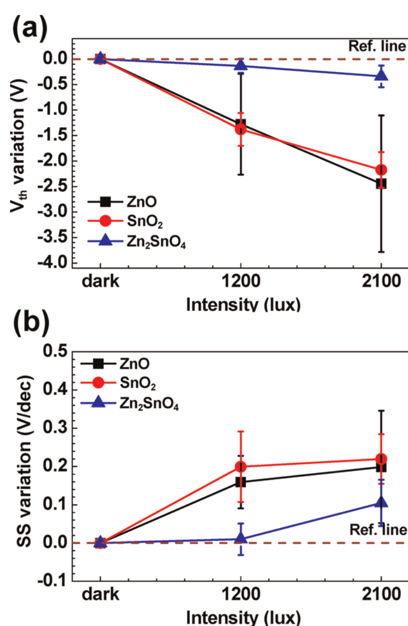

Figure 6. (a) V_{th} variation *versus* intensity and (b) subthreshold slope variation *versus* intensity for ZnO, SnO_2, and Zn_2SnO_4 nanowire transistors.

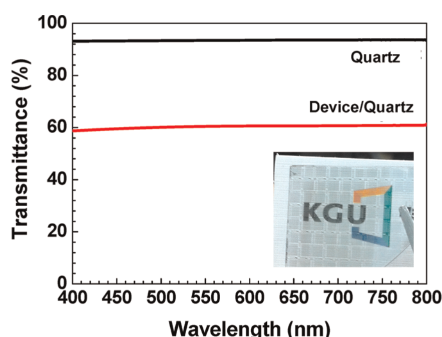

Figure 7. Optical transmission spectra of Zn_2SnO_4 nanowire transistors on a quartz substrate.

the nanowires is not prompt. Actually, the decay time tends to increase in vacuum due to lack of oxygen to react.[43]

A comprehensive understanding of the photostability of the Zn_2SnO_4 nanowire requires detailed nanostructural and electronic structural information which are not currently available. However, according to Chen *et al.*,[44] Sn doping on ZnO thin films causes the reduction of structural defects in ZnO, and two free electrons are generated as Sn^{4+} ions substitute Zn^{2+} ion sites.[45] In other words, Sn doping causes the decrease of structural defects and the increase of free electrons. Considering that photocurrent generation uses oxygen molecules and defects on the nanowire surface as a vehicle and is affected by carrier generation, it is assumed that the structural defects including oxygen vacancy of Zn_2SnO_4 decrease and finally lead to photocurrent reduction in comparison to ZnO or SnO_2.

On the basis of the above discussion, spinel Zn_2SnO_4 nanowires are assumed to be more stable than ZnO and SnO_2 nanowires under the same lighting conditions because fewer defects are generated during the growth phase. This well-known mechanism in play for the ZnO and SnO_2 nanowires in Figure 4a,b is suppressed for the Zn_2SnO_4 nanowires. The changes of V_{th} and SS values of ZnO, SnO_2, and Zn_2SnO_4 nanowire transistors were examined through 10 rounds of three-stage light illumination cycle (0−1200−2100 lx). Figure 5 shows the changes in V_{th} and SS extracted from the $I_{ds}-V_{gs}$ curves of ZnO, SnO_2, and Zn_2SnO_4 nanowire transistors while 0, 1200, and 2100 lx of light was applied 10 times, respectively. The transistor characteristics indeed changed in a repetitive and consistent manner according to three levels of illumination. In the case of ZnO nanowire transistors, changes in V_{th} and SS exhibited reproducibility. The shift amount of V_{th} was −1.7 V, and the change of SS was ∼0.28 V/dec from the initial stage at 1200 lx. Likewise, the shift amount V_{th} was −3.5 V, and the change of SS was ∼0.38 V/dec from the initial stage at 2100 lx. Besides, V_{th} and SS values could not be perfectly recovered to the original points with the lamp off (Figure 5a,d). SnO_2 nanowire transistors also showed reproducible behavior according to three different intensities of illumination. As indicated in the figures, the shift amounts of V_{th} were −1.3 and −2.0 V from the initial stage at 1200 and 2100 lx. The changes of SS were ∼0.12 and ∼0.22 V/dec from the initial stage at 1200 and 2100 lx. Here also, the V_{th} and SS values could not be recovered to the original points with the lamp off (Figure 5b,e). It is noted that the V_{th} and SS changes of SnO_2 nanowire transistors were smaller than those of ZnO nanowire transistors. On the other hand, Zn_2SnO_4 nanowire transistors showed the smallest change of V_{th}, −0.3 and −0.4 V negative shift from the initial stage at 1200 and 2100 lx. The devices also showed consistent SS characteristics regardless of the three different stages of illumination (Figure 5c,f).

The changes of V_{th} and SS in ZnO, SnO_2, and Zn_2SnO_4 due to illumination variation were measured in six nanowire transistors, and the average and standard deviations are shown in Figure 6. When the intensity increased from 0 to 2100 lx, the V_{th} of ZnO and SnO_2 showed -2.4 ± 1.3 and -2.2 ± 0.3 V negative shifts, respectively. On the other hand, Zn_2SnO_4 produced only 0.34 ± 0.22 V of negative shift, which is relatively a slight change. Meanwhile, as for SS changes, ZnO and SnO_2 increased by 0.2 ± 0.15 and 0.22 ± 0.07 V/dec, respectively, whereas Zn_2SnO_4 increased by 0.10 ± 0.06 V/dec, showing no significant change under varied light illumination conditions. These results suggest that Zn_2SnO_4 nanowire transistors are more suitable for transparent displays because of their stability and much smaller changes in their

electrical characteristics or SS compared with ZnO or SnO_2 nanowires under light illumination.

In order to prove the possibility of application to transparent displays, we fabricated a transparent Zn_2SnO_4 nanowire transistor on a transparent quartz substrate using the same process and measured the transmittance shown in Figure 7. The black and red lines correspond to quartz and Zn_2SnO_4 nanowire transistors, respectively. The inset is the image of a transparent Zn_2SnO_4 nanowire transistor substrate showing that the text on the paper behind the substrate is visible. The quartz substrate exhibited ~91% transmittance, whereas the transistor substrate using Al/ITO as source-drain showed ~60% transmittance. For reference, the transistor characteristics of devices fabricated on the quartz substrate were similar to those of devices fabricated on the Si wafer.

CONCLUSIONS

In summary, we have synthesized Zn_2SnO_4 nanowires showing stability against external illumination for applications in transistors used for transparent and/or flexible displays. The Zn_2SnO_4 nanowires were found to have a cubic crystalline structure. The electrical characteristics of ZnO and SnO_2 nanowires under light illumination were also analyzed for comparison. Among the changes caused by external illumination in the characteristics of ZnO and SnO_2 nanowire transistors, a negative shift in V_{th} and an increasing trend in the SS were clearly observed. However, such changes in the case of Zn_2SnO_4 nanowire transistors were much lower in comparison. Moreover, the Zn_2SnO_4 nanowires returned to their initial state immediately after the light source was removed, whereas the ZnO and SnO_2 nanowires failed to be restored even ~10 min after the light source was removed. The results here conclude that the use of Zn_2SnO_4 nanowires remarkably enhances the photostability of the transistors compared to ZnO and SnO_2 nanowires, and Zn_2SnO_4 is a potential alternative to conventional oxide and amorphous or polysilicon that can operate stably in transparent displays without additional processing.

METHODS

Single-crystalline Zn_2SnO_4 nanowires were grown by chemical vapor deposition on SiO_2/Si substrates uniformly coated with 20 nm gold nanoparticles as catalyst. A mixture of ZnO (99.999%, 0.6 g) and SnO (99.99%, 1.5 mol %, 0.0149 g) was used as source material. The temperatures of the source and substrate zones in the quartz tube reactor were 1090 and 720 °C, respectively. A mixed carrier gas (Ar + 1.6% O_2) was passed through the tube at a rate of 60 sccm for 1 h. Single-crystalline ZnO and SnO_2 nanowires were also grown for comparison on SiO_2/Si substrates uniformly coated with 20 nm gold nanoparticles. Identical conditions were used for ZnO nanowires except for twice the carrier gas flow rate. The SnO_2 nanowires were grown using a SnO source material with the two zones maintained at 850 and 700 °C and the mixed carrier gas (Ar + 2% O_2) at a rate of 100 sccm for 30 min. The as-grown nanowires were analyzed using field emission scanning electron microscopy (FE-SEM), high-resolution transmission electron microscopy (HR-TEM), photoluminescence (PL) spectroscopy, and X-ray diffraction (XRD). A He–Cd laser (Kimon, 1 K, Japan) with a wavelength of 325 nm and a power of 50 mW was utilized as an excitation source for PL measurement.

Bottom-gated transistors were fabricated to evaluate the device performance using Zn_2SnO_4, ZnO, and SnO_2 nanowires. The fabrication process consisted of gate electrode formation, gate insulator deposition, contact hole formation, nanowire dispersion, and source/drain electrode formation. The detailed process is as follows: First, we rinsed a thermally grown SiO_2/Si wafer and quartz wafer substrates. Sputtered indium tin oxide (ITO, 100 nm) was deposited on top of the substrates. ITO gate electrodes were then formed by patterning through the lift-off method. Al_2O_3 (30 nm, $\varepsilon \sim 9$) was deposited to form a gate insulator by atomic layer deposition. A contact hole was created on the gate electrode pad areas *via* etching to probe the gate metals. Next, the nanowires were uniformly dispersed on the substrates. The as-grown nanowires were separated from the growth substrate by placing it into VLSI-grade 2-propanol solution subjected to ultrasonication. Then, a few drops of this suspension of nanowires was disbursed on the patterned substrate in order to form the channel, followed by cleaning off the residual liquid and dust using deionized (DI) water. Both ends of the dispersed nanowires were contacted by the source/drain electrodes, which were deposited as a double layer of 50 nm thick aluminum and 70 nm thick indium tin oxide (ITO) by sputtering and patterned to complete the fabrication of the nanowire transistors. This double layer serves to reduce the contact resistance and maintain an adequate level of reliability on the repetitive measurements. The transistor transfer characteristics, including hysteresis with and without light sources, were evaluated. Three levels of illumination intensity, 0 (dark), 1200, and 2100 lx were supplied by a halogen lamp (12 V, 100 W), and we compared mainly the threshold voltage (V_{th}, V_{gs} at I_{ds} = 1 nA, V_{ds} = 0.5 V) and subthreshold slope (SS).

Conflict of Interest: The authors declare no competing financial interest.

Acknowledgment. This research was supported by the National Research Foundation of Korea (NRF) funded by the Ministry of Education, Science and Technology (2011-0023219, 2011-0019133, and 2011K000627). The World Class University program at POSTECH funded by the Ministry of Education, Science and Technology through the National Research Foundation of Korea (R31-10100) is also acknowledged.

REFERENCES AND NOTES

1. Ju, S.; Facchetti, A.; Xuan, Y.; Liu, J.; Ishikawa, F.; Ye, P.; Zhou, C.; Marks, T. J.; Janes, D. B. Fabrication of Fully Transparent Nanowire Transistors for Transparent and Flexible Electronics. *Nat. Nanotechnol.* **2007**, *2*, 378–384.
2. Huitema, H. E. A.; Gelinck, G. H.; van der Putten, J. B. P. H.; Kuijk, K. E.; Hart, C. M.; Cantatore, E.; Herwig, P. T.; van Breemen, A. J. J. M.; de Leeuw, D. M. Plastic Transistors in Active-Matrix Displays. *Nature* **2001**, *414*, 599.
3. Chen, Y.; Au, J.; Kazlas, P.; Ritenour, A.; Gates, H.; McCreary, M. Flexible Active-Matrix Electronic Ink Display. *Nature* **2003**, *423*, 136.
4. Gelinck, G. H.; Huitema, H. E. A.; van Veenendaal, E.; Cantatore, E.; Schrijnemakers, L.; van der Putten, J. B. P. H.; Geuns, T. C. T.; Beenhakkers, M.; Giesbers, J. B.; Huisman, B.-H.; *et al.* Flexible Active-Matrix Displays and Shift Registers Based on Solution-Processed Organic Transistors. *Nat. Mater.* **2004**, *3*, 106–110.
5. Ko Park, S.-H.; Hwang, C.-S.; Jeong, H. Y.; Chu, H. Y.; Cho, K. I. Transparent ZnO-TFT Arrays Fabricated by Atomic Layer Deposition. *Electrochem. Solid-State Lett.* **2008**, *11*, H10–H14.

6. Lee, J.-H.; Kim, J.-H.; Han, M.-K. A New a-Si:H TFT Pixel Circuit Compensating the Threshold Voltage Shift of a-Si:H TFT and OLED for Active Matrix OLED. *IEEE Electron Device Lett.* **2005**, *26*, 897–899.
7. Tai, Y.-H.; Chen, B.-T.; Kuo, Y.-J.; Tsai, C.-C.; Chiang, K.-Y.; Wei, Y.-J.; Cheng, H.-C. A New Pixel Circuit for Driving Organic Light-Emitting Diode with Low Temperature Polycrystalline Silicon Thin-Film Transistors. *J. Display Technol.* **2005**, *1*, 100–104.
8. Park, K.; Jeon, J.-H.; Kim, Y.; Choi, J. B.; Chang, Y.-J.; Zhan, Z.; Kim, C. A Poly-Si AMOLED Display with High Uniformity. *Solid-State Electron.* **2008**, *52*, 1691–1693.
9. Choi, Y. J.; Lim, B. C.; Woo, I. K.; Ryu, J. I.; Jang, J. Low Photo-Leakage Current Amorphous Silicon Thin Film Transistor with a Thin Active Layer. *J. Non-Cryst. Solids* **2000**, *266*–*269*, 1299–1303.
10. Liang, C.-Y.; Gan, F.-Y.; Liu, P.-T.; Yeh, F. S.; Chen, S. H.-L.; Chang, R.-C. A Novel Self-Aligned Etch-Stopper Structure with Lower Photo Leakage for AMLCD and Sensor Applications. *IEEE Electron Device Lett.* **2006**, *27*, 978–980.
11. Liu, X.; Wu, X.; Cao, H.; Chang, R. P. H. Growth Mechanism and Properties of ZnO Nanorods Synthesized by Plasma-Enhanced Chemical Vapor Deposition. *J. Appl. Phys.* **2004**, *95*, 3141–3147.
12. Mahalingam, T.; Lee, K. M.; Park, K. H.; Lee, S.; Ahn, Y.; Park, J.-Y.; Koh, K. H. Low Temperature Wet Chemical Synthesis of Good Optical Quality Vertically Aligned Crystalline ZnO Nanorods. *Nanotechnology* **2007**, *18*, 035606.
13. Huang, M. H.; Wu, Y.; Feick, H.; Tran, N.; Weber, E.; Yang, P. Catalytic Growth of Zinc Oxide Nanowires by Vapor Transport. *Adv. Mater.* **2003**, *13*, 113–116.
14. Lin, B.; Fu, Z.; Jia, Y. Green Luminescent Center in Undoped Zinc Oxide Films Deposited on Silicon Substrates. *Appl. Phys. Lett.* **2001**, *79*, 943–945.
15. Liu, J.; Lee, S.; Ahn, Y. H.; Park, J.; Koh, K. H. Tailoring the Visible Photoluminescence of Mass-Produced ZnO Nanowires. *J. Phys. D: Appl. Phys.* **2009**, *42*, 095401.
16. Cross, R. B. M.; De Souza, M. M.; Sankara Narayanan, E. M. A Low Temperature Combination Method for the Production of ZnO Nanowires. *Nanotechnology* **2005**, *16*, 2188–2192.
17. Morhain, C.; Teisseire-Doninelli, M.; Vezian, S.; Deparis, C.; Lorenzini, P.; Raymond, F.; Guion, J.; Neu, G. Near Band Edge Emission of MBE Grown ZnO Epilayers: Identification of Donor Impurities and O_2 Annealing Effects. *Phys. Status Solidi B* **2004**, *241*, 631–634.
18. Sun, X. H.; Lam, S.; Sham, T. K.; Heigl, F.; Jurgensen, A.; Wong, N. B. Synthesis and Synchrotron Light-Induced Luminescence of ZnO Nanostructures: Nanowires, Nanoneedles, Nanoflowers, and Tubular Whiskers. *J. Phys. Chem. B* **2005**, *109*, 3120–3125.
19. Zhu, Y.; Chen, Y.; Zhang, X. Study on the Annealing-Dependent Photoluminescence Properties of SnO_2 Cluster-System Structures. *Eur. J. Chem.* **2011**, *2*, 8–13.
20. Kim, H. W.; Shim, S. H. Branched Structures of Tin Oxide One-Dimensional Nanomaterials. *Vacuum* **2008**, *82*, 1395–1399.
21. Hu, J.; Bando, Y.; Liu, Q.; Golberg, D. Laser-Ablation Growth and Optical Properties of Wide and Long Single-Crystal SnO_2 Ribbons. *Adv. Funct. Mater.* **2003**, *13*, 493–496.
22. Wang, L.; Zhang, X.; Liao, X.; Yang, W. A Simple Method To Synthesize Single-Crystalline Zn_2SnO_4 (ZTO) Nanowires and Their Photoluminescence Properties. *Nanotechnology* **2005**, *16*, 2928–2931.
23. Jie, J.; Wang, G.; Han, X.; Fang, J.; Yu, Q.; Liao, Y.; Xu, B.; Wang, Q.; Hou, J. G. Growth of Ternary Oxide Nanowires by Gold-Catalyzed Vapor-Phase Evaporation. *J. Phys. Chem. B* **2004**, *108*, 8249–8253.
24. Chen, H.; Wang, J.; Yu, H.; Yang, H.; Xie, S.; Li, J. Transmission Electron Microscopy Study of Pseudoperiodically Twinned Zn_2SnO_4 Nanowires. *J. Phys. Chem. B* **2005**, *109*, 2573–2577.
25. Wang, S.; Yang, Z.; Lu, M.; Zhou, Y.; Zhou, G.; Qiu, Z.; Wang, S.; Zhang, H.; Zhang, A. Coprecipitation Synthesis of Hollow Zn_2SnO_4 Spheres. *Mater. Lett.* **2007**, *61*, 3005–3008.
26. Lei, M.; Kwong, F.-L.; Ng, D. H. L. Synthesis of Zn_2SnO_4 Nanowires and Their Photoluminescence Properties. *J. Nanosci. Nanotechnol.* **2010**, *10*, 8432–8437.
27. Deng, R.; Zhang, X. T. Effect of Sn Concentration on Structural and Optical Properties of Zinc Oxide Nanobelts. *J. Lumin.* **2008**, *128*, 1442–1446.
28. Lv, H.; Sang, D. D.; Li, H. D.; Du, X. B.; Li, D. M.; Zou, G. T. Thermal Evaporation Synthesis and Properties of ZnO Nano/Microstructures Using Carbon Group Elements as the Reducing Agents. *Nanoscale Res. Lett.* **2010**, *5*, 620–624.
29. Hu, Q. R.; Jiang, P.; Xu, H.; Zhang, Y.; Wang, S. L.; Jia, X.; Tang, W. H. Synthesis and Photoluminescence of Zn_2SnO_4 Nanowires. *J. Alloys Compd.* **2009**, *484*, 25–27.
30. Lin, H.-F.; Liao, S.-C.; Hung, S.-W.; Hu, C.-T. Thermal Plasma Synthesis and Optical Properties of Zn_2SnO_4 Nanopowders. *Mater. Chem. Phys.* **2009**, *117*, 9–13.
31. Zhao, J.-W.; Qin, L.-R.; Zhang, L.-D. Single-Crystalline Zn_2SnO_4 Hexangular Microprisms: Fabrication, Characterization and Optical Properties. *Solid State Commun.* **2007**, *141*, 663–666.
32. Wang, J.; Sun, X. W.; Xie, S.; Zhou, W.; Yang, Y. Single-Crystal and Twinned Zn_2SnO_4 Nanowires with Axial Periodical Structures. *Cryst. Growth Des.* **2008**, *8*, 707–710.
33. Wang, J. X.; Xie, S. S.; Gao, Y.; Yan, X. Q.; Liu, D. F.; Yuan, H. J.; Zhou, Z. P.; Song, L.; Liu, L. F.; Zhou, W. Y.; Wang, F. Growth and Characterization of Axially Periodic Zn_2SnO_4 (ZTO) Nanostructures. *J. Cryst. Growth* **2004**, *267*, 177–183.
34. Chen, D.; Xu, J.; Liang, B.; Wang, X.; Chen, P. C.; Zhou, C.; Shen, G. Electric Transport, Reversible Wettability and Chemical Sensing of Single-Crystalline Zigzag Zn_2SnO_4 Nanowires. *J. Mater. Chem.* **2011**, *21*, 17236–17241.
35. Pang, C.; Yan, B.; Liao, L.; Liu, B.; Zheng, Z.; Wu, T.; Sun, H.; Yu, T. Synthesis, Characterization and Opto-Electrical Properties of Ternary Zn_2SnO_4 Nanowires. *Nanotechnology* **2010**, *21*, 465706.
36. Soci, C.; Zhang, A.; Xiang, B.; Dayeh, S. A.; Aplin, D. P. R.; Park, J.; Bao, X. Y.; Lo, Y. H.; Wang, D. ZnO Nanowire UV Photodetectors with High Internal Gain. *Nano Lett.* **2007**, *7*, 1003–1009.
37. Park, S.-H. K.; Hwang, C.-S.; Ryu, M.; Yang, S.; Byun, C.; Shin, J.; Lee, J.-I.; Lee, K.; Oh, M. S.; Im, S. Transparent and Photo-Stable ZnO Thin-Film Transistors To Drive an Active Matrix Organic-Light-Emitting-Diode Display Panel. *Adv. Mater.* **2009**, *21*, 678–682.
38. Zhang, Y.; Wang, J.; Zhu, H.; Li, H.; Jiang, L.; Shu, C.; Hu, W.; Wang, C. High Performance Ultraviolet Photodetectors Based on an Individual Zn_2SnO_4 Single Crystalline Nanowire. *J. Mater. Chem.* **2010**, *20*, 9858–9860.
39. Kar, A.; Stroscio, M. A.; Meyyappan, M.; Gosztola, D. J.; Wiederrecht, G. P.; Dutta, M. Tailoring the Surface Properties and Carrier Dynamics in SnO_2 Nanowires. *Nanotechnology* **2011**, *22*, 285709.
40. Keem, K.; Kim, H.; Kim, G. T.; Lee, J. S.; Min, B.; Cho, K.; Sung, M. Y.; Kim, S. Photocurrent in ZnO Nanowires Grown from Au Electrodes. *Appl. Phys. Lett.* **2004**, *84*, 4376–4378.
41. Heo, Y. W.; Kang, B. S.; Tien, L. C.; Norton, D. P.; Ren, F.; La Roche, J. R.; Pearton, S. J. UV Photoresponse of Single ZnO Nanowires. *Appl. Phys. A: Mater. Sci. Process.* **2005**, *80*, 497–499.
42. Chen, Y.; Zhu, C.; Cao, M.; Wang, T. Photoresponse of SnO_2 Nanobelts Grown *in Situ* on Interdigital Electrodes. *Nanotechnology* **2007**, *18*, 285502.
43. Li, Q. H.; Gao, T.; Wang, Y. G.; Wang, T. H. Adsorption and Desorption of Oxygen Probed from ZnO Nanowire Films by Photocurrent Measurements. *Appl. Phys. Lett.* **2005**, *86*, 123117.
44. Chen, K. J.; Hung, F. Y.; Chen, Y. T.; Chang, S. J.; Hu, Z. S. Surface Characteristics, Optical and Electrical Properties

on Sol–Gel Synthesized Sn-Doped ZnO Thin Film. *Mater. Trans.* **2010**, *51*, 1340–1345.

45. Vaezi, M. R.; Sadrnezhaad, S. K. Improving the Electrical Conductance of Chemically Deposited Zinc Oxide Thin Films by Sn Dopant. *Mater. Sci. Eng., B* **2007**, *141*, 23–27.